JSEE Vol. 22, No. 1, 2020 DOI:10.48303/jsee.2020.244168

Prediction of Ultimate Capacity of Welded Steel Moment Connections under Extremely Low Cycle Fatigue and Progressive Collapse

Mohsen Ghaderi[1], Mohsen Gerami[2*], and Reza Vahdani[3]

1. Ph.D. Graduate, Researcher of Civil Engineering, Semnan University, Semnan, Iran
2. Professor of Civil Engineering, Semnan University, Semnan, Iran,
*Corresponding Author; email: mgerami@semnan.ac.ir
3. Assistant Professor of Civil Engineering, Semnan University, Semnan, Iran

Received: 21/05/2019
Accepted: 29/05/2021

ABSTRACT

In order to determine the performance level of steel structures or to strengthen them, it is necessary to determine the ultimate capacity of their connections under the influence of extremely low cycle fatigue caused by cyclic load. On the other hand, the ultimate capacity or failure of the connections, under unavoidable monotonic loadings such as explosions or fires, needs to be determined in order to predict the progressive collapse in structures utilizing intermediate and/or special moment frames. In this study, the ultimate capacity of welded connections, subjected to monotonic loading, is estimated using the Stress Modified-Critical Strain model (SMCS). However, the Cyclic Void Growth Model (CVGM) is used to investigate connection capacity under cyclic loading. These models could be used to estimate the ultimate capacity of connections to determine the performance levels of the structures where it is not practical or possible to test laboratory specimens. In this paper, the ultimate capacity of connections are obtained based on the crack initiation criterion in three types of moment connections, namely reduced beam section (RBS), welded unreinforced flange-welded web (WUF-W), and increased beam section (IBS) moment connections; (1) subjected to monotonic loading in the column removal scenario by using the (SMCS) model, and (2) under cyclic loading by using the (CVGM). This research shows that by using the ductile fracture models, it is possible to predict the ultimate capacity and fracture mode of the welded moment connections with great accuracy. The results of this investigation, using fracture models, indicate that out of the three types of connections, the seismic rotational capacity of the IBS moment connection is the largest (0.05 radians), next is RBS (0.044 radians), and WUF-W is the last (0.04 radians) with the least rotational capacity under cyclic loading. The results also reveal that the rotation capacity of the connections under monotonic loading is two to three times the capacity of the same connection under cyclic loading (IBS:0.20 radians, RBS: 0.16 radians and WUF-W :0.147 radians).

Keywords:
Ultimate capacity;
Ductile fracture;
Monotonic loading;
Cyclic loading;
CVGM model; SMCS model

1. Introduction

Although structures are designed for possible incidents during their service life, recent events such as the destruction of structures in the Northridge earthquake of 1994 [1], the Kobe earthquake of 1995 [2], the collapse of the World Trade Center in the United States during attacks in 2001, and the collapse of Plasco Shopping Tower in Iran due to fire in 2017 showed that structures may face disasters more severe than their design levels over their lifetime. These events clearly revealed the limitations in recognizing the true behavior of steel structures under progressive collapse [3-4].

Often, destruction in a structure is due to the fracture in its main members. Fracture in steel structures during the Northridge (1994) and Kobe (1995) earthquakes lead to researchers shifting their attention to the fracture phenomenon in structures [5-6]. In the Kobe earthquake, more than 100 moment frames had experienced severe cracking and/or fracture in the beam-column connections and more than 30 buildings had suffered overall or partial destruction [7].

Today, recognizing the causes and effects of general and partial fracture in structures is one of the important engineering needs. One of the parameters that make the study of the collapse difficult is the lack of laboratory tests on structural member fractures, and therefore, verification of the proposed fracture models is hard. Current fracture models in steel structures generally use a constant critical strain to detect member fractures [3, 4, 8].

In the steady-state critical strain method, the onset of fracture occurs when the strain reaches a certain value in the member; therefore, the effects of the ductile fracture that are dependent on the triaxial stresses are not considered in this method. The steel material used in the building industry usually exhibits a ductile fracture with large plastic deformations. The observed stages during steel fracture in buildings include the void formation, the void growth, and the coalescence of voids [9].

Rice and Tracy [10] suggested that the growth of voids was often in more than one direction and is also strongly influenced by the triaxial stress values and triaxial stress states. Hancock and Mackenzie [11] concluded that the onset of the ductile rupture in a material depends on the interaction of the triaxial stresses and the plastic strains. If the triaxial stress increases, then the critical strain decreases. This constitutes the basis of the stress modified critical strain model (SMCS), which is used to evaluate the ductile fracture under monotonic loading. The (SMCS) model is based on the assumption that the triaxial stress does not change during strain increase and it is only considered in the current state with no regards to the stress history [9].

In order to evaluate the structure fractures under cyclic load, the Cyclic Void Growth Model was proposed by Kanvinde and Deierlein [12] in 2008. The Cyclic Void Growth Model (CVGM) is capable of estimating the extremely low cycle fatigue (ELCF) process based on the simulation of void cyclic growth accumulation and its integration with progressive damage to materials with intermediate voids. In fact, the (CVGM) model is an extension of the void growth model, which aims to overcome the void growth process by considering the triaxial state of stresses [13-14].

Due to the lack of proper laboratory facilities, the capacity of moment connections has been evaluated only within the range of about 0.04 radians of connection rotation (required by AISC Seismic Provisions) and just a few laboratory studies have investigated connection rotations up to the onset of fracture and/or rupture of the connection plates. Sadek et al. [15] used the column removal scenario to study the ultimate capacity and the manner in which connection fracture in reduced beam section (RBS) connections under monotonic loading occurs. Then, using a constant strain model, they modeled the connection fracture with ABAQUS software [16]. Lee et al. [17] conducted experiments on RBS connections and evaluated the fracture and ultimate capacity of the connections under cyclic loading.

The yield and ultimate rotation capacity of RBS and WUF-W moment connections, presented in FEMA-350 [18], is based on experiments in most of which the testing had been stopped when the connections began to yield and hence, connection fracture never actually took place.

In this research, it has been tried to determine the ultimate connection capacity and/or connection failure that is generally used to determine the performance levels of structures. In addition, by using the ductile fracture mechanics models based on the crack initiation and propagation criteria, fracture process in reduced beam section (RBS), welded unreinforced flange-welded web (WUF-W), and increased beam section (IBS) moment connections are investigated; (1) under cyclic loadings (like earthquake), and (2) progressive failure under monotonic loading. Thus, in cases where it is not practical or possible to carry out laboratory experiments to evaluate steel moment connection ultimate capacity and fracture, the behavior of structures can be predicted - when it is subjected to destruction caused by earthquake or fire - by using the ductile fracture theories.

2. Ductile Fracture Mechanism

Under the monotonic tensile loading, the onset of the ductile fracture is due to the growth of micro-voids and coalescence of voids, which in turn, is due to the plastic strain and the triaxial stresses on the micro-voids. The basic hypothesis is that the ductile fracture will start when the volume of micro-voids reaches a critical value. There are two main differences between fracture mechanisms under cyclic loading and monotonic loading. First, the void growth under monotonic tensile loading will be progressive, while under cyclic loading, the repeated reversals of triaxial stresses would cause the voids to expand and contract [12]. Second, due to the cumulative damage to the voids under cyclic loading, the critical size of the voids is smaller than that under monotonic loading, which may cause faster coalescence of voids and faster fracture in the material [12].

Steel structures exposed to severe earthquakes experience extremely low cycle fatigue, i.e. ELCF is a failure mode in which large plastic strains are applied to the structure in a very small number of cycles (less than 10 to 20 cycles). ELCF is completely different from low cycle fatigue and high cycle fatigue that is characterized by thousands and millions of cycles. The ELCF is an interaction of fracture-fatigue mechanism that forms a ductile fracture and was first suggested by Kawamora and Yamamota [19] and further verified by Kanvinde and Deierlein [12]. Three-dimensional images of extremely small cracks show that the ductile fracture in steel structures usually consists of three stages of micro-void nucleation, growth, and coalescence [20].

3. Stress Modified Critical Strain for Monotonic Loading

According to Rice and Tracy [10], Hancock and Mackenzie [11], and Kanvinde and Deierlein [13], the void growth model (VGM) was developed under monotonic loading. For a spherical void in an infinite continuous environment, the void growth rate under monotonic tensile loading can be expressed by Equation (1) [21-22]:

$$dr / r = C \exp(1.5T)\, d\varepsilon_p \tag{1}$$

where r is the instantaneous radius of the spherical cavity, C is the material constant, $T = \frac{\delta_m}{\delta_e}$ is the triaxial stress. δ_m is the average stress and δ_e is the effective stress (Von Mises stress). $d\varepsilon_p = \sqrt{(2/3) d\varepsilon_{ij}^p d\varepsilon_{ij}^p}$ is the incremental equivalent plastic strain. By integrating Equation (1), the total void growth (the ratio of the void radius to the initial radius) over a period of tensile plastic stress is expressed in Equation (2):

$$\ln(r / r_0) \int_0^{\varepsilon^p} C \exp(1.5T)\, d\varepsilon_p \tag{2}$$

Assuming that the void growth controls the stages of fracture, the ductile fracture begins when the void growth rate reaches the critical level determined by Equation (3):

$$\ln(r / r_0)^{critical}_{monotonic} = \int_0^{\varepsilon_p^{critical}} C \exp(-1.5T) d\varepsilon_p \tag{3}$$

where, $\varepsilon_p^{critical}$ represents the critical plastic strain while fracture is due to coalescence. Equation (3) is divided by the material constant C to give $\eta_{monotonic}$ as:

$$\eta_{monotonic} = \frac{\ln(r / r_0)^{critical}_{monotonic}}{C} = \int_0^{\varepsilon^{p\ critical}} \exp(1.5T)\, d\varepsilon_p \tag{4}$$

where $\eta_{monotonic}$ represents the void growth capacity and is characterized by the stiffness of the material determined by the critical void growth rate.

The failure criterion based on the fracture index under monotonic loading is given by Equation (5):

$$FI_{monotonic} = \int_0^{\varepsilon^{p\ critical}} \exp(1.5T)\, d\varepsilon_p / \eta_{monotonic} \tag{5}$$

where, $FI_{monotonic}$ shows the ratio of void growth demand to the void growth capacity. When computed value of $FI_{monotonic}$ is above unity, the start of fracture is expected.

The Rice and Tracy's VGM model includes an explicit term for integrating triaxial stresses and plastic strains. However, in many realistic (material) situations, the material deformation is so large that the triaxial stresses can be ignored (which depends on the geometry of the material). Even if the rate of change of strain is very high, this may still be true. In most cases, the triaxial stress is independent of the plastic strain. As a result, the term inside the integral in Equation (2) emanates from the integral and the

VGM model is represented by Equation (6):

$$\ln\left(\frac{R}{R_0}\right)_{monotonic}^{critical} = C\exp(1.5T).d\varepsilon_p^{critical} \quad (6)$$

Therefore, the critical plastic strain can be expressed as follows:

$$\varepsilon_p^{critical} = \frac{\ln\left(\frac{R}{R_0}\right)_{monotonic}^{critical}}{C\exp(1.5T)} = \frac{\ln\left(\frac{R}{R_0}\right)_{monotonic}^{critical}}{C}\exp(1.5T) \quad (7)$$

It is clear from Equation (7) that the two terms are related to the base coefficient of the material and can be replaced with a material parameter called α:

$$\alpha = \frac{\ln\left(\frac{R}{R_0}\right)_{monotonic}^{critical}}{C} \quad (8)$$

Equation (8) is the basis of the (SMCS) model and the basis of Hancock's explanation [11], which concluded that the initiation point of the material's ductile rupture depends on the interaction of the triaxial stresses and the plastic strains. If the triaxial stress increases, the critical value of the plastic strain decreases. This is mathematically shown in Equation (9), which is the Equation of the (SMCS) model.

$$\varepsilon_p^{critical} = \alpha\exp(-1.5T) \quad (9)$$

4. Cyclic Void Growth Model

Equation (1) can be modified to give Equation (10) for the reversible cyclic loading [9].

$$dr / r = sign(T)\ C\exp(-1.5T)d\varepsilon_p \quad (10)$$

where the term sign (T) takes into account the direction of the triaxial stresses T.

According to Equation (10), if the triaxial stress (T) is positive, the voids will expand under the plastic strain and if T is negative, the voids will shrink. The values of the triaxial stress and the equivalent plastic strain determine whether the voids would grow or shrink.

The integration of Equation (10) will continue in the tensile and compressive loading intervals up to the onset of fracture. The critical value of the accumulated void growth by cyclic strains can be shown as in Equation (11):

$$\ln(r / r_0)^{critical}_{cyclic} = \sum_{tensile} C_1\int_{\varepsilon_1}^{\varepsilon_2}\exp(|1.5T|)\,d\varepsilon_p - \sum_{compressive} C_1\int_{\varepsilon_1}^{\varepsilon_2}\exp(|1.5T|)\,d\varepsilon_p \quad (11)$$

The size of the voids will increase during positive triaxial stresses and will decrease during negative triaxial stresses. The first term on the right side of Equation (11) indicates the sum of the growth of the voids in all cycles due to the positive triaxial stresses which requires the calculation of the integral in the plastic strain intervals of ε_1 and ε_2 at the beginning and the end of each tensile stage. The second term on the right side of the equation shows the sum of the shrinkage of the voids in all cycles due to the negative triaxial stresses. The terms $C1$ and $C2$ are constants that are used to indicate the difference between the void growth rate and contraction rate.

Due to the lack of information on the void growth rate and contraction rate, it is assumed that $C1 = C2 = C$ [9]. Dividing Equation (11) by C, the material constant, η_{cyclic} is given as:

$$\eta_{cyclic} = \frac{\ln(r / r_0)^{critical}_{cyclic}}{C} = \sum_{tensile}\int_{\varepsilon_1}^{\varepsilon_2}\exp(|1.5T|)\,d\varepsilon_p - \varepsilon_1 \sum_{compressive}\int_{\varepsilon_1}^{\varepsilon_2}\exp(|1.5T|)\,d\varepsilon_p \quad (12)$$

where η_{cyclic} represents the void growth capacity under cyclic loading which is obtained by reducing the corresponding value under the monotonic loading as shown in Equation (13):

$$\eta_{cyclic} = \frac{\ln(r / r_0)^{critical}_{cyclic}}{C} = \exp(-\lambda\varepsilon_c)\frac{\ln(r / r_0)^{critical}_{monotonic}}{C} = \exp(-\lambda\varepsilon_c)\eta_{monotonic} \quad (13)$$

λ is a coefficient that depends on the material vulnerability and is obtained by using cyclic and

monotonic tests of materials along with finite element analysis [12]. And ε_c is the damage variable defined as the compressive equivalent plastic strain, determined by the sum of all plastic strains in compression cycles under loadings. In Equation (13), an exponential decay function is used to reduce the "material capacity under monotonic loading" in order to obtain the "material capacity under cyclic loading".

In accordance with Equation (12), the void growth demand; VGD_{cyclic}, under cyclic loading is determined by Equation (14).

$$VGD_{cyclic} = \sum_{tensile} \int_{\varepsilon_1}^{\varepsilon_2} \exp(|1.5T|) - \sum_{compressive} \int_{\varepsilon_1}^{\varepsilon_2} \exp(|1.5T|) \geq 0 \quad (14)$$

VGD_{cyclic} will alternately increase and decrease under cyclic loading; however, the negative volume of the void has on meaning, so the VGD_{cyclic} must always be positive. Therefore, when the result of Equation (14) drops below zero, the VGD_{cyclic} value must remain zero until it rises to above zero in the tensile cycles. Similar to the tensile cyclic loading, ELCF fracture under cyclic loading occurs when the volume of voids (VGD_{cyclic} demand) exceeds the volume of void growth capacity η_{cyclic}. In other words, when $FI_{cyclic} \geq 1$, fracture will follow. The term FI_{cyclic} is defined by Equation (15).

$$FI_{cyclic} = \frac{VGD_{cyclic}}{\eta_{cyclic}} \quad (15)$$

Therefore, the CVGM model used to predict the ELCF fracture in materials subject to very high-amplitude cyclic loading is based on the fact that the void growth demand, VGD_{cyclic}, increases simultaneously as the void growth capacity, η_{cyclic}, is reduced by the cumulative damage of the materials [22-23].

5. Research Methodology

In this research, it is tried to predict the ultimate capacity of RBS, WUF-W and IBS moment connections under cyclic and monotonic loadings using ductile fracture theories and mathematical models. These models may be used to predict the behavior of structures subjected to destruction, when laboratory testing of connections is not possible. First, the results of experiments conducted by Sadek et al. [15] and Sykin et al. [24], (in which they used the column removal scenario to examine the capacity of RBS connections under monotonic loading) is used to verify the accuracy of the Stress Modified-Critical Strain (SMCS) model. With regards to checking the efficacy of Cyclic Void Growth Model (CVGM), the connection tested by Lee et al. [17] is modeled and evaluated. Having made sure that the ductile fracture models, under cyclic and monotonic loadings, perform reasonably well, five RBS, 4 WUF-W, and 2 IBS moment connections are modeled, using ABAQUS software [16], and their rotation capacities under monotonic and cyclic loadings are evaluated by sub-routines of SMCS and CVGM fracture models in ABAQUS software.

IBS is a type of moment connection where instead of weakening the beam section, it is made stronger near the column and is connected to the column by direct welding. IBS is suitable for use with built up I-beams. In this type of connections, frame displacement problems associated with RBS connections are resolved. Therefore, two IBS-type moment connections are included in this research.

By using ABAQUS software and the fracture process the rotation capacity of the three types of connections are investigated.

6. Verification under Monotonic Loading and Void Growth and Coalescence Theory

To ensure the correctness of results of this paper, the simplified monotonic void growth model (SMCS), used in the study of ductile fracture in welded steel moment connections by Sadek et al. [15] (which was further verified in Sykin' Ph.D. thesis [24] at Boston University), is first modeled in this paper by using ABAQUS software. In tests conducted by Sadek et al. [15], the column removal scenario was used in a frame consisting of three columns and two beams. The parameters of the simplified VGM model or SMCS, were calculated according to Ph.D. thesis of Saykin et al. [24]. The value or for steel material A992 is 0.62. The frame's beam and column dimensions and the material specifications are given in Table (1). The load was applied to the middle column of the structure in the form of displacement, varying linearly from 0 to 860 mm, in the vertical direction.

Table 1. RBS connection in the research conducted by Sadek et al. [15].

Member	Member Dimensions (mm)	Material	Yield Stress (MPa)	Ultimate Stress (MPa)
BEAM (w24×94) h×b×t×s	617×230×13×23	A992	445	554
COLUMN (W24×131) h×b×t×s	621×326×15×24	A992	378	494

According to Sadek et al. [15], the failure first occurred in the lower flange of the beam, near the middle column, at displacement of 851 mm and was then expanded into the web. The rotation tolerated in the beam at the onset of failure was 0.14 radians, Figure (1). The specimen modeled by Sadek et al. [15] and that modeled in this paper are shown in Figures (2) and (3), respectively. The results of ABAQUS model of this paper shows the occurrence of beam failure at displacement of 851 mm and rotation of 0.14 radians see (Figure 4). The vertical displacement of the middle column against the horizontal displacement of the side columns, from Sadek's research, and this research is plotted in Figure (5). A good consistency between the two is observed.

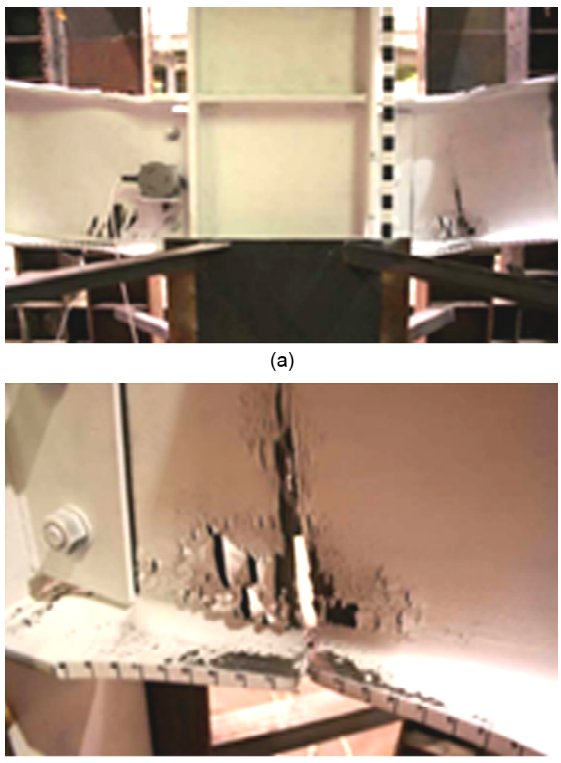

(a)

(b)

Figure 1. (a and b) The failure of the RBS connection at drift of 14% and displacement of 851 mm- tested by Sadek et al. [15].

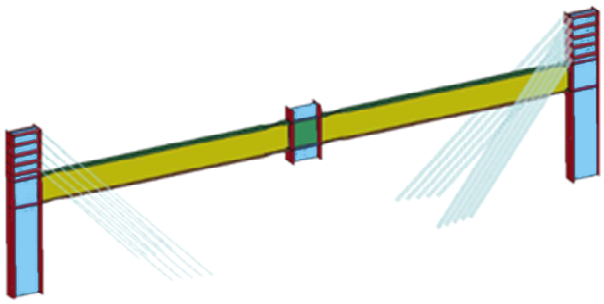

Figure 2. The frame modeled by Sadek et al. [15].

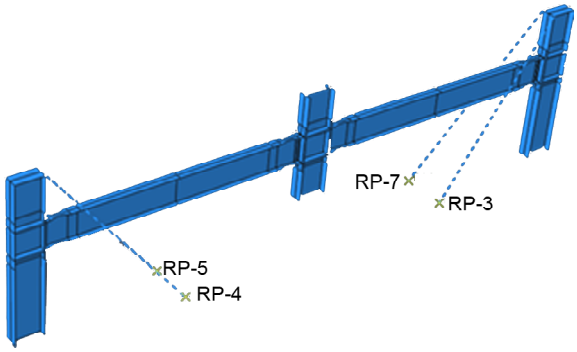

Figure 3. The frame modeled in ABAQUS, for verification purposes.

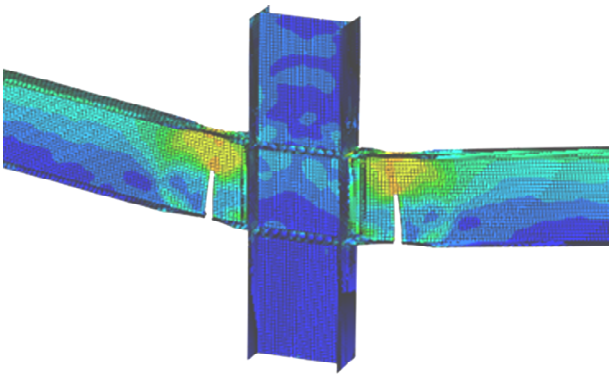

Figure 4. The frame failure at the displacement of 851 mm and drift of 14%.

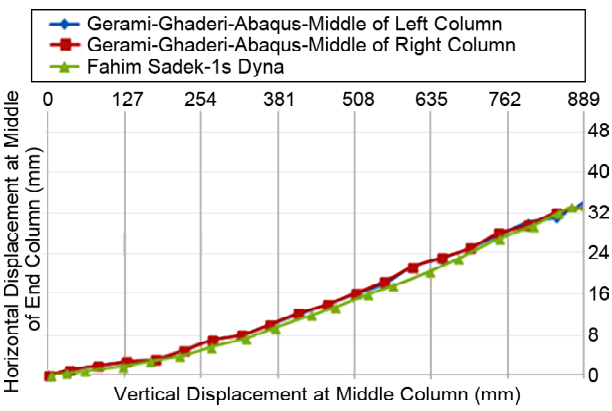

Figure 5. Conformity of the modeling in this study with the model reported by Sadek et al. [15] - the horizontal displacement of the side columns against the vertical displacement of the middle column.

7. Verification under Cyclic Loading and Extremely Low Cycle Fatigue Theory

To ensure that the use of cyclic void growth model (CVGM) in the study of the extremely low cycle fatigue (ELCF), in the welded connections of steel moment frames produces acceptable results, the connection from Lee et al.'s paper [17] was modeled by ABAQUS in this paper. CVGM parameters were obtained using UVARM subroutine and the quantities λ and $\eta_{monotonic}$ for the reduced beams were selected as 1.25 and 2.5, respectively, as suggested by Meyer et al. [25-26]. The specifications of the beam and column in the connection are given in Table (2). The loading is applied to the structure according to tests from Lee et al. [17], which in turn is based on SAC loading as shown in Figure (6).

Based on the results of Lee's paper, failure will occur in the first drift cycle of 6%, Figure (7).
The results of finite element analyses (prepared for verification purposes), Figure (8), and plot of FI_{cyclic} values, Figure (9), both show that at the end of the first drift cycle of 6%, the FICYCLIC value has exceeded unity; i.e., failure occurs. It is evident in Figure (10) that in cycle 67, at the end of the first drift cycle of 6%, the value of VGD_{cyclic} exceeds η_{cyclic}, indicating the onset of fracture.

Table 2. The specifications of the beam and column in the RBS connection in Lee et al.'s research [17].

Member	Member Dimensions (mm)	Material	Yield Stress (MPa)	Ultimate Stress (MPa)
BEAM h×b×t×s	950×424×24×43	A992	345	424
COLUMN (Box) h×b×t×s	914×610×50×50	A572	420	490

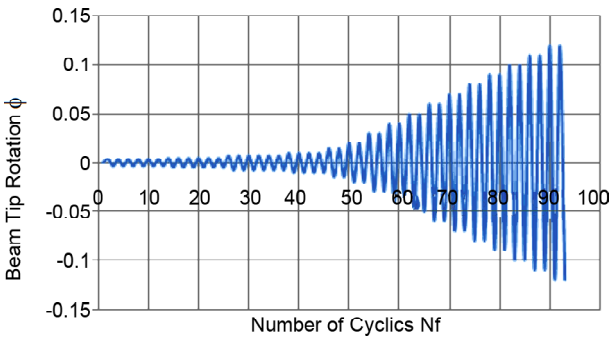

Figure 6. SAC loading protocol [17].

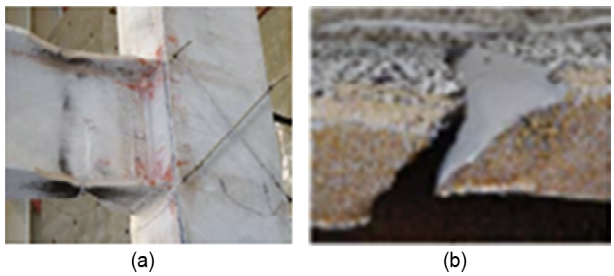

Figure 7. (a) RBS connection at 6% drift and (b) fracture in the upper flange at first cycle of 6% drift [17].

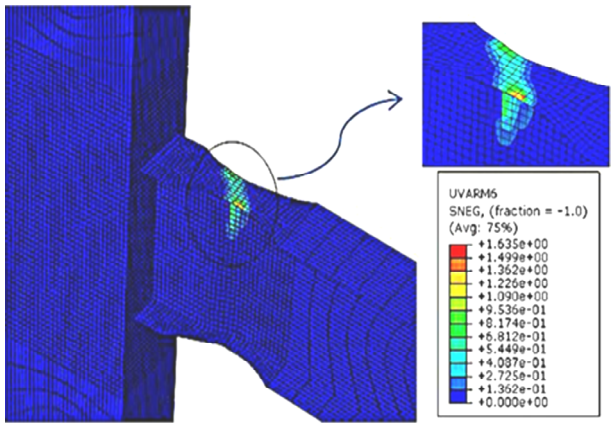

Figure 8. Failure in the verification specimen in the first drift cycle of 6%.

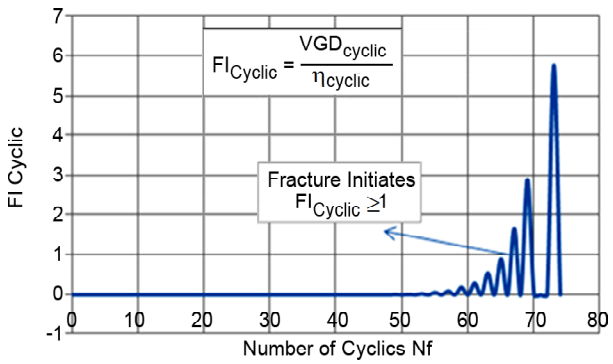

Figure 9. Failure start cycle in the verification specimen based on FI_{cyclic}.

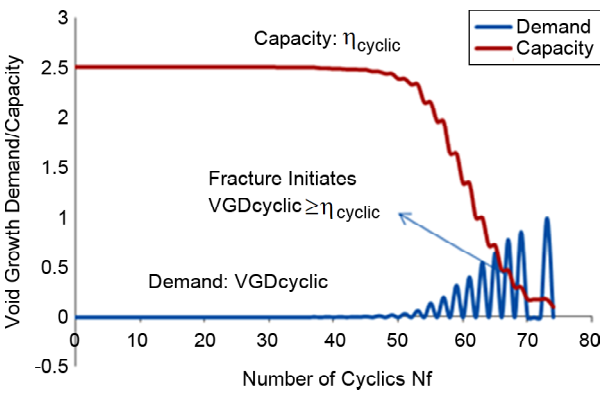

Figure 10. Failure start cycle in the verification specimen based on intersections of curves η_{cyclic} and VGD_{cyclic}.

8. Investigation of the Capacity of RBS, WUF-W, and IBS Connections under Monotonic Loading

The column removal scenario (of Sadek et al. [15] which was used to verify this research) is employed to investigate the capacity of RBS, WUF-W and IBS connections under monotonic loading. Five RBS, 4 WUF-W, and two IBS connections are modeled in ABAQUS software using SHELL elements. In addition to the connection rotation capacity, the location and onset of cracking and/or failure in the connections are examined. In Figure (11), the RBS connection detail modeled for loading in the column removal scenario is depicted. Table (3) lists the beams, columns, and RBS dimensions of the connections. The focus of study in each RBS specimen is presented in Table (4). Figure (11) shows the parametric dimensions of the RBS connection and Figure (12) displays a specimen of the RBS connection modeled in ABAQUS software, under the column removal scenario.

The specifications of the four WUF-W connection specimens modeled in this study are presented in Table (5). To consider the effects of welding access hole on the beam web, for each specimen, whether rolled or built-up I section, a welding access hole is modeled, see Figure (13).

A specimen of WUF-W connection modeled in ABAQUS software for the column removal scenario is presented in Figure (13).

Table (6) shows the dimensions of the beams, columns, and increased areas of two IBS connections modeled in this paper. The proposed IBS connection modeled by ABAQUS software is shown in Figure (14a). Figure (14b) indicates the parametric dimensions of the IBS connections as

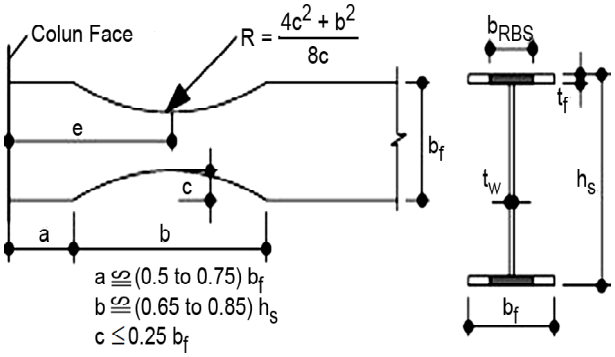

Figure 11. RBS moment connection dimensions according to AISC regulations, showing parameters a, b, c, r [17].

Table 3. Dimensions of RBS specimens.

	Member Dimensions h×b×t×s (mm)	RBS Dimensions a	b	c	r
1	Beam 400×350×10×30	262.5	395	52.5	400
	Column 400×350×12×30				
2	Beam 400×350×10×50	262.5	395	52.5	400
	Column 400×350×12×30				
3	Beam 1000×350×20×30	262.5	700	52.5	1200
	Column 1000×350×12×30				
4	Beam 1000×350×20×30	262.5	700	52.5	1200
	Column 1000×350×12×30				
5	Beam 1000×350×20×30	265.5	700	49.5	1200
	Column 1000×350×12×30				

Table 4. Focus of study in each RBS specimen.

Specimen No	The Objective for Specimen Analysis
1	Monitoring the location of the plastic hinge formations = a + b / 2 and examining the length of a + b, the protected area
2	The effect of increasing the thickness of the flange of the reduced beam to a thickness of 50 mm
3	Checking the depth of beam up to 1 m and the depth of column up to 1 m with the lateral side restraint and the beam length-to-depth ratio of 9
4	The depth of the beam up to 1 m and the depth of the column up to 1 m with lateral side restraint and the beam length-to-depth ratio of 6
5	Investigating the effect of varying parameters a and c of specimen 3

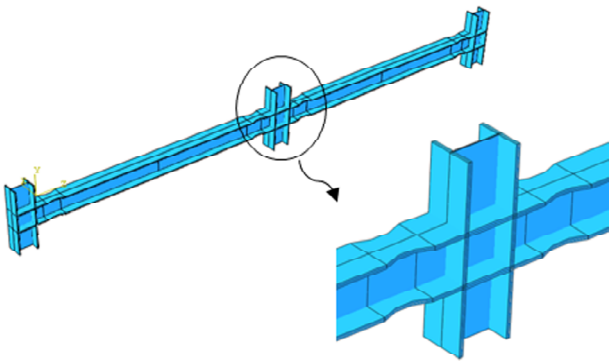

Figure 12. RBS connection modeled in ABAQUS.

Table 5. Specifications of WUF-W specimens.

	Member Dimensions h×b×t×s (mm)	Type of Weld Access Hole
1	Beam 400×350×10×30 / Column 400×350×12×30	Rolled I Beams or Built up I Sections Welded Prior to Creating Access Hole
2	Beam 400×350×10×50 / Column 400×350×12×30	Built up I Section
3	Beam 1000×350×20×30 / Column 1000×350×12×30	Rolled I Beams or Built Up I Sections Welded Prior to Creating Access Hole
4	Beam 1000×350×20×30 / Column 1000×350×12×30	Built Up I Section

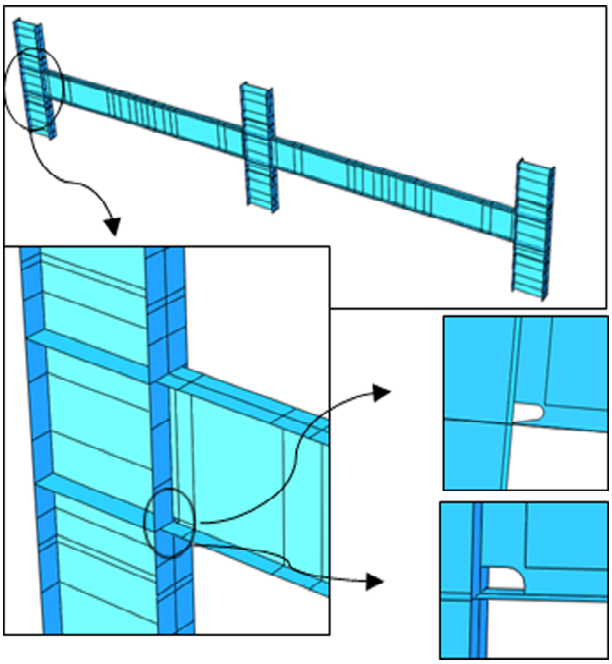

Figure 13. WUF-W connection and two specimens of access holes in two ABAQUS models.

Table 6. Dimensions of IBS specimens.

Specimen Number	Member Dimensions h×b×t×s (mm)	Dimensions of Increased Area			
		a	b	c	r
1	Beam 400×240×10×30	262.5	197	52.5	400
	Column 400×350×12×30				
2	Beam 1000×240×10×50	262.5	197	52.5	400
	Column 1000×350×20×30				

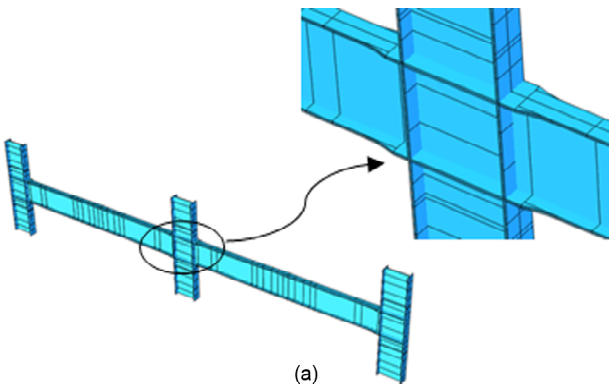

Figure 14a. The IBS connection modeled in ABAQUS.

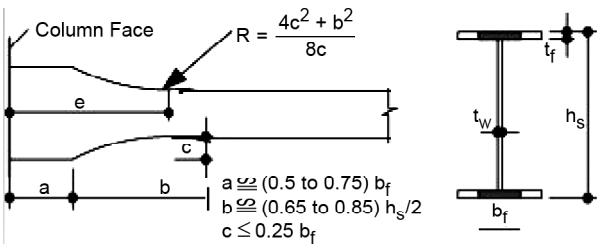

Figure 14b. IBS connection, displaying parameters a, b, c and r.

required by AISC Regulations. The major advantage of IBS connection is the increased connection stiffness, which results in smaller frame deflections as opposed to RBS moment connections. Its only disadvantage is that it cannot be used with rolled I beams.

To investigate the capacity of connections under monotonic loading, they are all analytically tested according to Sadek's scenario [15], where the middle column is displaced downwards until failure occurs. The parameters of the simplified VGM, and SMCS models were obtained on the basis of the Saykin et al. [24] and Kanvinde and Deierlein [12-14]. The value of α or $\eta_{monotonic}$ for ST-37 steel is selected as 2.44, which corresponds to steel grade with properties closest to that of ST-37.

Middle column displacements, beam lengths, and rotation capacity of RBS connections under monotonic loading and column removal scenario, is listed in Table (7). Crack initiation in the middle of RBS bottom flange at connection rotation of 0.17 radians, for specimen No. 1 is indicated in Figure (15).

In Figures (15) to (19), the location of crack initiation and rupture in the modeled RBS connections, under the column removal scenario, are shown. As depicted in the figures, in all five connections, the onset of cracking occurs at the center of the reduced area of the lower flange and propagates into the connection web. The average rotation of the five connections is 0.161 radians. The analytical testing of the five RBS connections to failure under monotonic loading indicates that:

1. The connection rotation capacity decreases with increasing the depth of the beam (reduction of connection rotation capacity of specimens 3 to 5 as compared to specimens 1 and 2).
2. By comparing specimen 2 with specimen 1, it is

Table 7. Connection rotation capacity under the column removal scenario in RBS connections.

Specimen No.	The Beam Length (m)	At the Onset of Crack Initiation	
		Middle Column Displacement (mm)	Connection Rotation (radians)
1	6	1025	0.17
2	6	1025	0.17
3	9	1425	0.158
4	6	975	0.162
5	9	1300	0.147

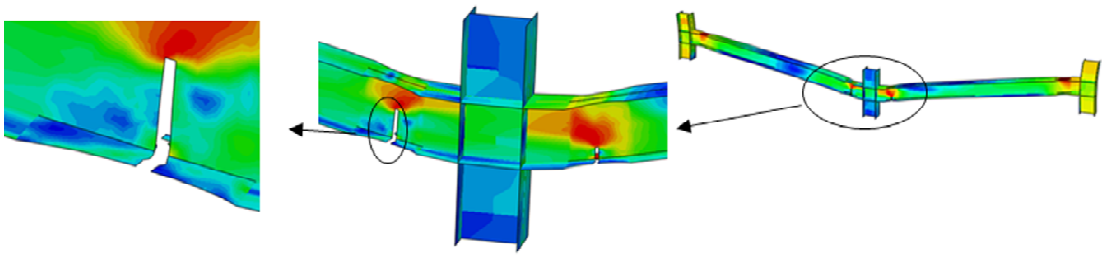

Figure 15. RBS moment connection, specimen No 1 under column removal scenario - the crack initiation location in the middle connection.

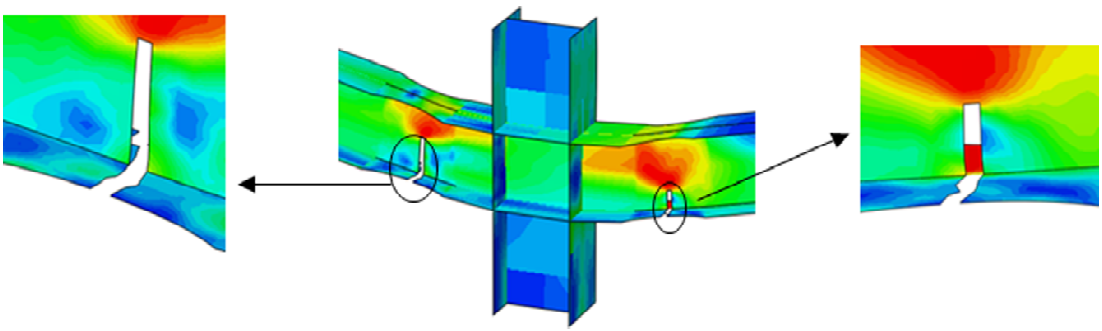

Figure 16. The crack initiation point in the connection type 2.

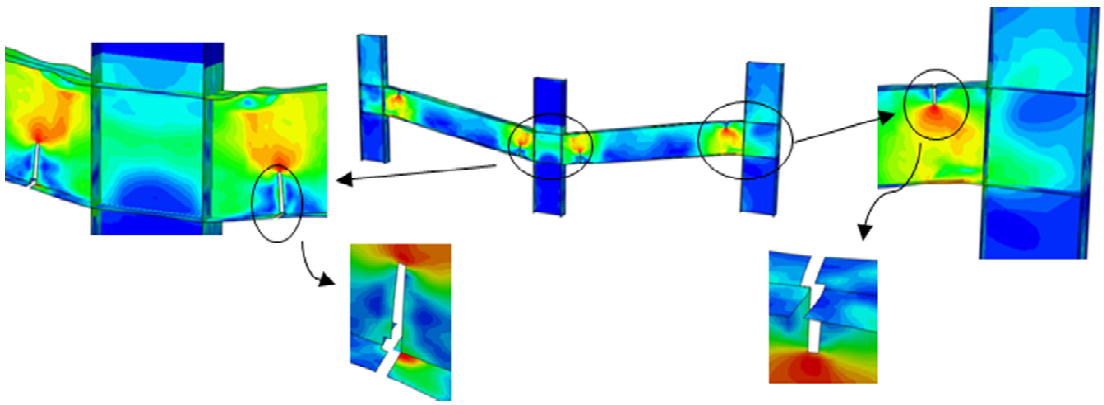

Figure 17. The crack initiation point in the connection type 3.

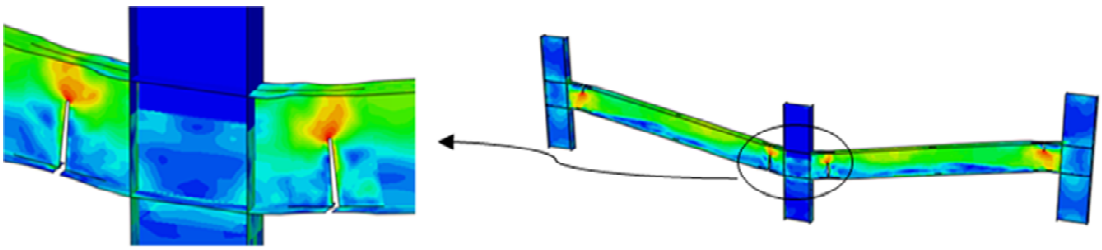

Figure 18. The crack initiation point in the connection type 4.

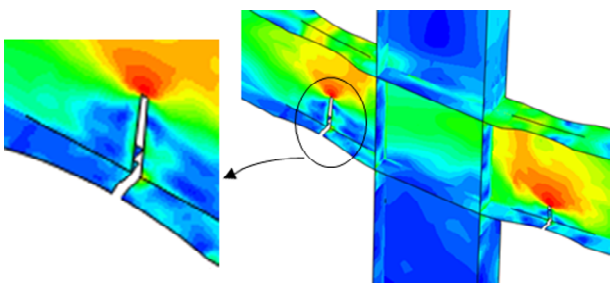

Figure 19. The crack initiation point in the connection type 5.

found that increasing the thickness of the beam flange within the limits of the AISC Regulations has no effects on the rotation capacity of the connections.

3. The connection rotation capacity decreases with decreasing the beam section reduction (comparison of specimen 5 with specimen 3).
4. Comparing specimens 3 and 5 with specimen 4 indicates that increasing the beam length-to-depth ratio does not necessarily increase the rotation capacity of the beam.
5. Examination of the failure location in all the specimens shows that the crack initiation started at the center of the reduced area (of bottom flange due to downwards displacement of middle column), and therefore, the protected zone is exactly in agreement with the requirements of AISC Specifications.

Table (8) lists the rotation of the WUF-W connections, under monotonic loading and the column removal scenario, at the onset of cracking. In Figure (20), the modeled frame is shown for specimen No. 1. Also, the crack initiation in the connection, starts at the access hole at rotation of 0.154 radians.

A major disadvantage of WUF-W connections is the weld access holes; thus, all four WUF-W specimens (Table 5), containing access holes, are modeled in ABACUS. The analytical testing of the four WUF-W connections to failure under monotonic loading reveals that:

1. By increasing the beam depth from 400 mm to 1000 mm, the connection rotation capacity is reduced (comparison of specimens 1 and 2 with specimens 3 and 4).
2. WUF-W connections made of built-up I-section beams exhibit higher rotation capacity than connections made of rolled I beams with access holes (comparison of specimen 1 with 2 and specimen 3 with 4).

The onset of cracking in access holes of WUF-W specimens No. 3 and 4 (1000 mm beam depth) are shown in Figures (21) and (22) respectively.

Table (9) lists the beam lengths and the connection rotation under monotonic loading and the column removal scenario for the IBS connections. To investigate IBS connection rotation capacity, two specimens, listed in Table (6), are modeled in ABACUS. The main advantage of the IBS connection as compared to the RBS connection is that, due to the increase in the beam section at column connection, issues of frame displacement and reduced

Table 8. Rotation in WUF-W connections under the column removal scenario.

		Connection Rotation at the Onset of Cracking at	
Specimen	Beam Length (m)	Access Hole (radian)	Connection of Beam Flange to Column (radian)
1	6	0.154	0.154
2	6	0.16	0.16
3	8.825	0.1271	0.1388
4	8.825	0.135	0.1388

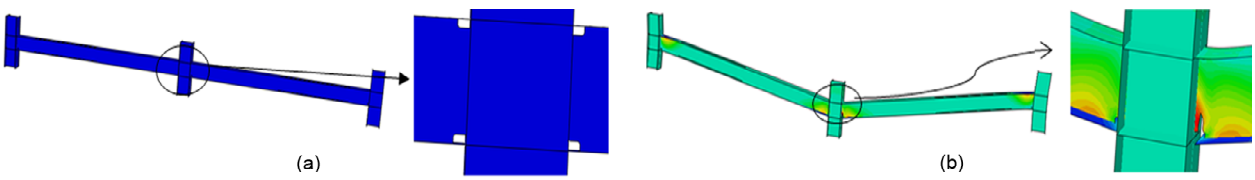

Figure 20. (a) Modeled WUF-W, specimen 1, under the column removal scenario and (b) The crack initiation location in the WUF-W connection at rotation of 0.154 radians.

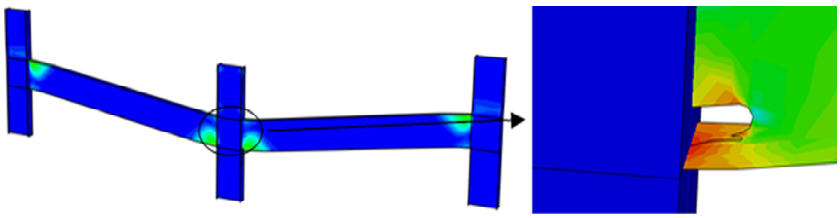

Figure 21. WUF-W connection, specimen 3, under the column removal scenario - start of failure in the WUF-W connection at rotation of 0.1271 radians at the rolled I beam access holes.

Table 9. Connection rotation of IBS connections under the column removal scenario.

		At the Onset of Crack Initiation	
Specimen No.	Beam Length (m)	Middle Column Displacement (mm)	Connection Rotation (radians)
1	6	1320	There is no fracture up to 0.22 radians
2	8.825	1791	There is no fracture up to 0.203 radians

beam strength associated with RBS connections are resolved.

As presented in Table (9), the IBS connection capacity has increased significantly compared to the RBS and WUF-W connections considered previously, and one of them has attained a rotation of 0.22 radians. Figure (23) shows the stress contours pertinent to the second IBS specimen.

It is noticed that, before commencement of failure, both IBS connections achieve a connection rotation of at least 0.20 radians. However, the highest plastic strain occurs in the beams, at the beginning of the enlarged flange, which verifies the transfer of plastic hinge, from column, to the beam.

9. Investigation of the Capacity of RBS, WUF-W, and IBS Connections under Cyclic Loading

To investigate the capacity of the RBS, WUF-W, and IBS moment connections under cyclic loading, the crack initiation in the connections is examined under SAC loading (Figure 6) (which is included in the commentary of the annex to the AISC) in order to determine the connection capacity under extremely low cycle fatigue [27-31]. The dimensions of RBS connection under examination are presented in Table (3). The subroutine UVARM is used to extract FI_{cyclic}. The λ and $\eta_{monotonic}$ values of ST-37 steel are selected as 1 and 2.5 respectively [32-33].

The column-cantilever beam model is used to evaluate the capacity of RBS, WUF-W, and IBS connections under cyclic loadings. Specifications of the columns and beams are exactly the same as those used for modeling under the column removal scenario [34]. The height of the free-standing columns is the same as the side columns used in the column removal scenario and the span of cantilevered beams is half the beam length of the models used for monotonic loading. Similar to monotonic loading case; five RBS, four WUF-W, and two IBS connections (one of each is shown in Figures (24) to (26) respectively) are modeled to investigate the connection capacities.

Table (10) shows the rotation of RBS connections modeled under cyclic loading. In Figure (27), the modeled frame of RBS specimen No. 1 under cyclic loading is shown. Also, the crack initiation in the RBS connection is indicated to occur in the

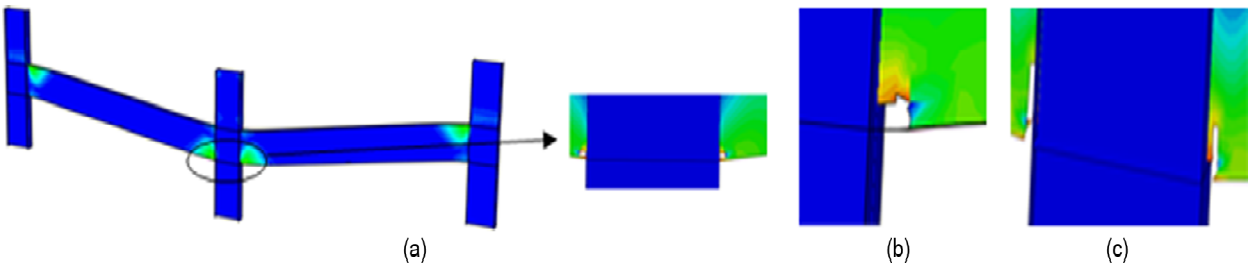

Figure 22. (a) WUF-W connection, specimen 4, before the start of crack, (b) the starting location of the failure crack at access hole and (c) the location of the failure crack at the connection of beam flange to column.

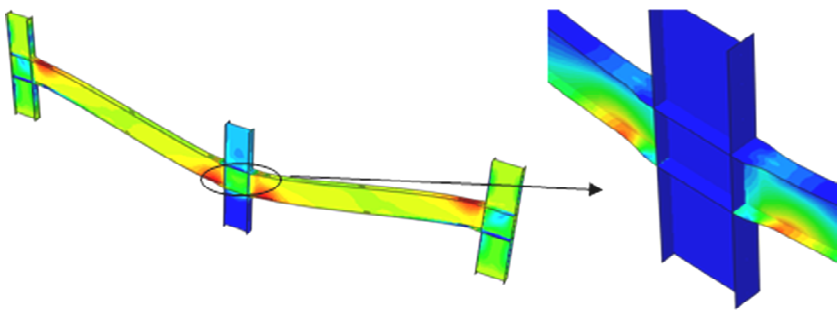

Figure 23. IBS connection - specimen No. 2 - No cracking seen up to rotation of 0.203 radians.

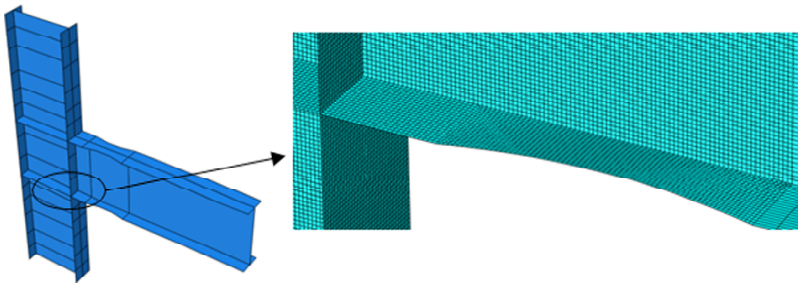

Figure 24. Cantilever model of RBS connection, specimen No. 3, mesh dimensions of 6 mm.

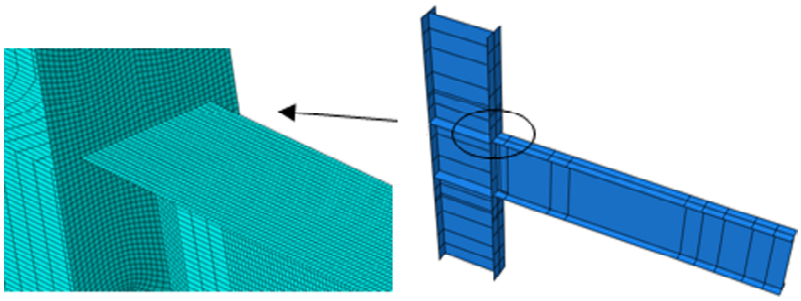

Figure 25. Cantilever model of WUF-W connection, specimen No. 3.

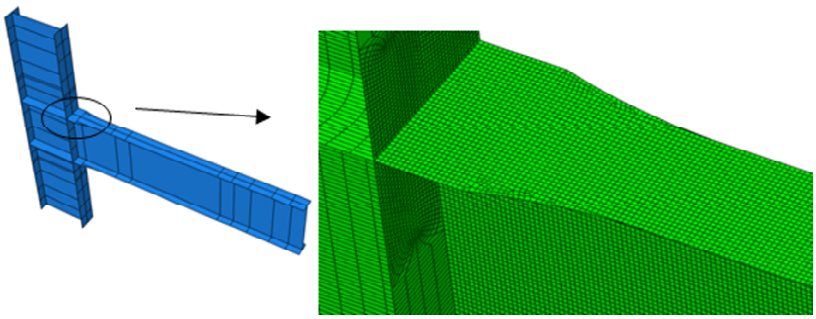

Figure 26. Cantilever model of IBS connection, specimen No. 2.

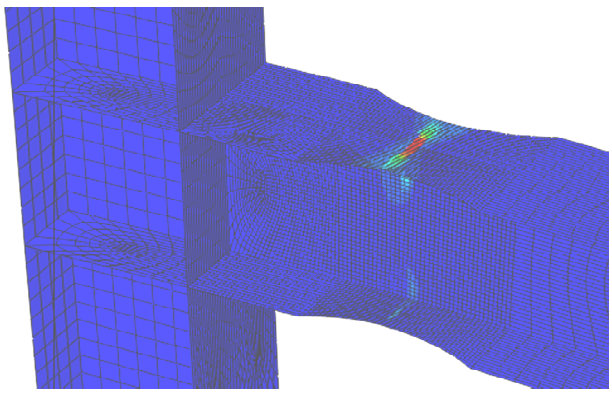

Figure 27. The location of crack initiation in the RBS connection of specimen No. 1 at rotation of 0.05 radians.

Table 10. Rotation of RBS connections subjected to cyclic loading.

Specimen No.	Beam Length (m)	The Location of Crack Initiation	Rotation in Frame Connections at the Time of Crack Initiation (rad)
1	3	The Center of Reduced Area	0.05 at 3rd Cycle
2	3	The Center of Reduced Area	0.06 at 1st Cycle
3	4.5	The Center of Reduced Area	0.04 at 2nd Cycle
4	3	Beam to Column Connection Location	0.03 at 4th Cycle
5	4.5	Beam to Column Connection Location	0.04 at 2nd Cycle

center of upper flange of the reduced beam at rotation of 0.05 radians.

Crack initiation in connections 1, 2, and 4, under cyclic loading, starts in the center of the reduced upper flange and propagates into the web. The average rotation of the first three connections is 0.05 radians. The analytical testing of the five RBS connections to failure under cyclic loading indicates that:

1. Increasing the beam depth, would result in a reduction in the connection capacity (reduction of the capacity of connections 3 and 5 compared to specimens 1 and 2).
2. By comparing specimen 2 with specimen 1, it is seen that increasing the thickness of the flanges, within the limits of the AISC Regulations, increases the rotation capacity of the connection.
3. Comparing the results of models 3 and 5 with model 4 indicates that increasing the beam length-to-depth ratio will cause an increase in the beam rotation capacity.
4. In models with deep beams, such as specimens 3 and 4, shear beam behavior becomes dominant. In other words, RBS efficiency is decreased and yielding zone is moved into the column area. However, the examination of specimen 1, 2, and 5 indicates that the crack initiation started at the center of the reduced beam, exactly in agreement with the provisions of AISC Specifications. Thus, further research on RBS connections with deep beams seems to be required.

Table (11) shows the rotation of the WUF-W connections modeled under cyclic loading. In Figure (28), the modeled frame of specimen 4 under cyclic loading is shown. Also, the crack initiation in the connection, at rotation of 0.03 radians, is indicated to start near the weld access hole.

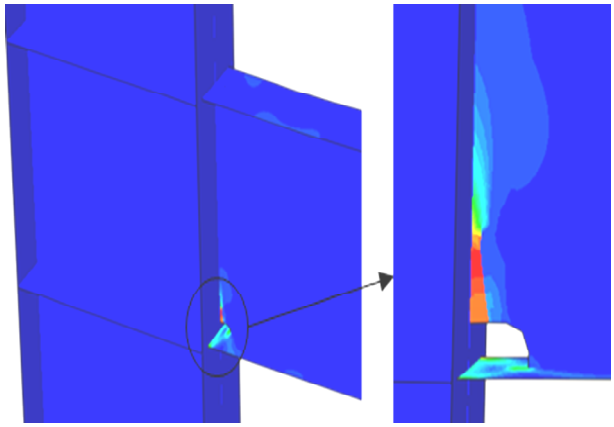

Figure 28. The crack initiation location in the WUF-W connection of specimen 4 at rotation of 0.03 radians.

The study of the WUF-W specimens under cyclic loading shows that the most vulnerable area in this type of connections, from viewpoint of crack initiation and propagation, is around the welding access holes. Also, by reviewing the results of Table (11), it is implied that (1) the access holes in rolled I-beams perform better than those in built-up I sections under seismic loading (comparing the capacity of specimens 1 and 3 with 2 and 4), and (2) with increasing the beam depth, the rotation capacity of the connection decreases significantly (comparison of specimens 1 and 2 with 3 and 4).

Table (12) lists the rotation of the IBS connections modeled under cyclic loading. In Figure (29), the modeled frame of specimen 1 under cyclic loading is depicted. In addition, the crack initiation in the IBS connection is indicated at rotation of 0.06 radians, at the beginning of the increased beam

Table 11. Rotation in WUF-W connections modeled under cyclic loading.

Specimen	Beam Length (m)	The Location of Crack Initiation	Connection Rotation at the Time of Crack Initiation (rad)
1	3	Access Hole	0.05 at 3rd Cycle
2	3	Access Hole	0.05 at 2nd Cycle
3	4.5	Near the Column Flange	0.03 at 2nd Cycle
4	4.5	Access Hole	0.03 at 1st Cycle

Table 12. Rotation of IBS connections modeled under cyclic loading.

Specimen No.	Beam Length (m)	The Location of Crack Initiation	Connection Rotation at the Time of Crack Initiation (rad)
1	3	beginning of the Increased Section	0.05 at 3rd Cycle
2	4.5	beginning of the Increased Section	0.06 at 1st Cycle

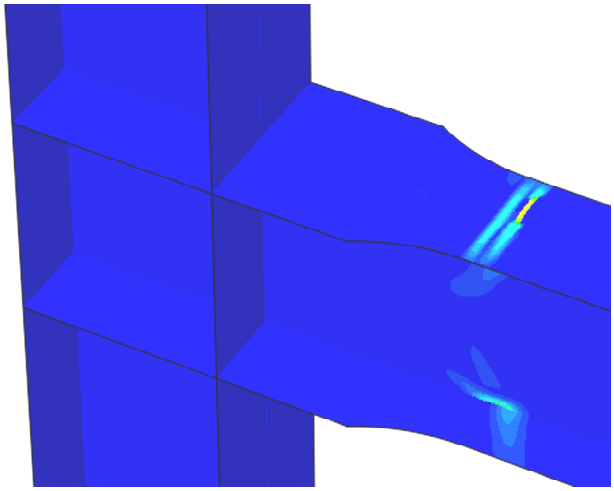

Figure 29. Crack initiation location in the IBS connection of specimen 1 at rotation of 0.06 radians.

section.

The investigation of IBS connections under cyclic loading shows that the rotation capacity of IBS connections is similar to that of RBS. Also, by examining the crack initiation in the IBS connections, it is suggested that the area in the beginning of the increased beam section is the most likely location for crack initiation to start in this type of connections. The results also reveal that with increasing the beam depth, the rotation capacity of the connection is reduced (comparison of specimen 1 with 2).

10. Comparison of the Capacity of Steel Welded Connections under Extremely Low Cycle Fatigue and Progressive Failure

The ultimate capacity of RBS connections under extremely low cycle fatigue is in the range of 0.03 to 0.06 radians. Under monotonic load and progressive failure, the capacity of this type of connection varies from 0.15 to 0.17 radians. The results obtained in this study are completely consistent with other research on the RBS connection [35-38]. Failure in most of the specimens occurs in the center of the reduced area. In Figure (30), the rotation capacities of the RBS specimens under monotonic and cyclic loadings are plotted.

The ultimate capacities of the WUF-W connections, subjected to cyclic loading, are in the range of 0.033-0.055 radians. The capacity of this type of connection under monotonic loading is estimated in the range of 0.138 to 0.16 radians. The failure of the specimens under cyclic and monotonic loading is observed to occur in the region of weld access holes. Figure (31) shows the plot of rotation capacities of the WUF-W specimens under monotonic and cyclic loadings.

The ultimate capacities in the IBS connections subjected to cyclic loading are in the range of 0.04 to 0.06 radians. The capacity of this type of connection under monotonic loading is estimated at 0.2 to 0.203 radians. The start of fracture in specimens under cyclic and monotonic loadings is seen at the beginning of the increased section in the beams. In Figure (32), the rotation capacities of IBS specimens under monotonic and cyclic loadings are compared.

The rotation capacities of RBS, WUF-W, and IBS connections are compared in Figure (33). It is observed that under monotonic loading, the IBS connection capacity is significantly higher than RBS, and WUF-W, with the latter having the least rotation capacity. The capacity of IBS and RBS connections under cyclic loading is approximately equal and are both greater than WUF-W.

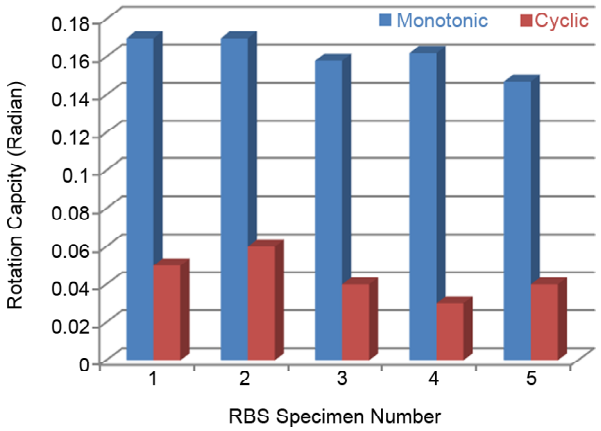

Figure 30. Comparison of the capacity of RBS specimens subjected to monotonic and cyclic loading.

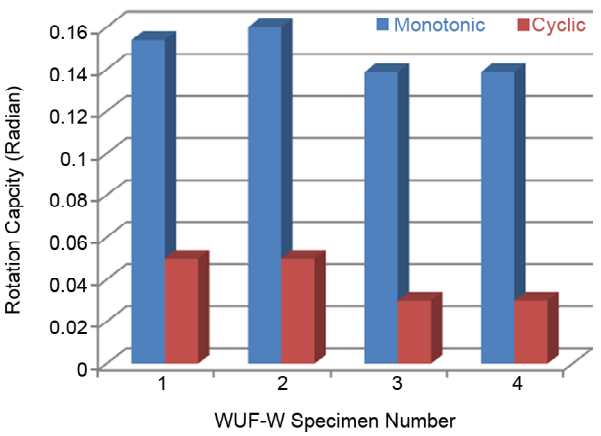

Figure 31. Comparison of the capacity of WUF-W specimens subjected to monotonic and cyclic loadings.

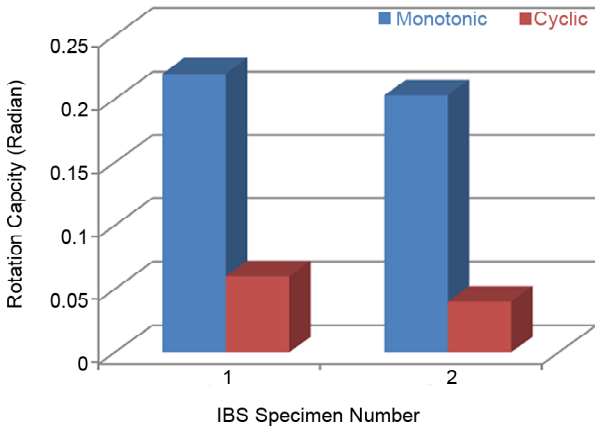

Figure 32. Comparison of the capacity of IBS specimens subjected to monotonic and cyclic loadings.

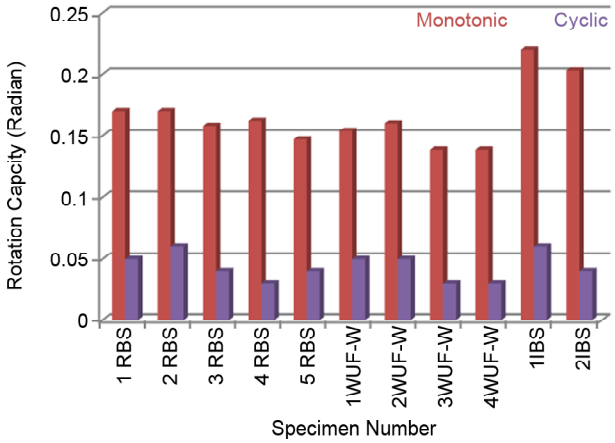

Figure 33. Comparison of the capacity of RBS, WUF-W, and IBS specimens subjected to monotonic and cyclic loadings.

11. Conclusions

In this research, by using fracture mechanics models, it was tried to determine the ultimate capacity (prior to failure) of RBS, WUF-W and IBS moment connections under cyclic loading, such as earthquakes, and under monotonic loadings, such as progressive failures. As a result, in cases where laboratory testing is not practical or possible, the ultimate capacity of the connections may be used to predict the behavior of structures and by use of ductile fracture theories and computer models failure may be predicted. In this regard, the connections were modeled using ABAQUS software, and the ductile fracture models under monotonic and cyclic loadings were utilized for this investigation.

This research shows that the ultimate capacity and fracture in structural welded connections may be predicted with high accuracy.

The results obtained on the basis of the ductile fracture models indicate that:

- The rotation capacity of the RBS, WUF-W, and IBS moment connections under monotonic loading is much higher than that under cyclic loading, and good performance of the welded connections under monotonic loading is observed.
- An average connection rotation of 0.2 radians was obtained for the IBS connection under monotonic loading in two modeled specimens. An average connection rotation of 0.16 radians was obtained for the RBS connection under monotonic loading in the five tested specimens. An average connection rotation of 0.1479 radians was obtained for the WUF-W connection under monotonic loading in the four tested specimens.
- In the RBS connections modeled under monotonic loading, cracking starts at the center of the reduced area of the lower flange and propagates to the web. In IBS connections modeled under monotonic loading, cracking starts at the beginning of the increased area of the lower flange and propagates to the web. Crack initiation in WUF-W connection under monotonic loading occurs around the weld access hole.
- The connection rotation capacity of RBS, WUF-W, and IBS connections, under monotonic loading, decreases with increasing the beam depth. In the investigated RBS connections, increasing the thickness of the beam flanges in the allowable range of AISC Regulations has no significant effect in the rotation capacity of the connection under monotonic loading.
- An average connection rotation of 0.044 radians was obtained for the five tested RBS connections under cyclic loading. An average connection rotation of 0.05 radians was obtained for the two tested IBS connections under cyclic loading. An average connection rotation of 0.04 radians was obtained for the four tested WUF-W connections under cyclic loading.
- In the welded connections modeled under cyclic loading, the connection rotation capacity decreases with increasing beam depth. In the RBS connections modeled under cyclic loading, increasing the thickness of the beam flanges within the allowable limits of the AISC Specifications produces an increase in the rotation capacity of the connection.

- Under monotonic loading, the rotation capacity of IBS is significantly higher than RBS connection, and last is WUF-W connection having the least capacity of them all. Under cyclic loading, IBS and RBS connection capacities are approximately equal and are both larger than WUF-W connection capacity.

Reference

1. Cooper, J.D., Friedland, I.M., Buckle, I.G., Nimis, R.B., and Bobb, N.M. (1994) *The Northridge Earthquake: Progress Made, Lessons Learned in Seismic-Resistant Bridge Design*. Report #58, U.S. DOT Federal Highway Administration, Washington, D.C.
2. Miyazaki, Y., Abe, K., Ando, M., et al. (2013) Seismic Activity in Japan, http://www.hp1039.jishin.go.jp/eqchreng/eqchrfrm.htm.
3. Khandelwal, K., El-Tawil, S., Kunnath, S.K., and Lew, H. (2008) Macromodel-based simulation of progressive collapse: steel frame structures. *Journal of Structural Engineering*, **7**(134), 1070-1078.
4. Szyniszewski, S. and Krauthammer, T. (2012) Energy flow in progressive collapse of steel framed buildings. *Engineering Structures*, **42**, 142-153.
5. Kuwamura, H. (2003) Classification of material and welding in fracture consideration of seismic steel frames. *Engineering Structures*, **5**(25), 547-563.
6. Kuwamura, H., Iyama, J., and Matsui, K. (2003) Effects of material toughness and plate thickness on brittle fracture of steel members. *Journal of Structural Engineering*, **11**(129), 1475-1483.
7. Kuwamura, H. and Yamamoto, K. (1997) Ductile crack as trigger of brittle fracture in steel. *Journal of Structural Engineering*, **6**(123), 729-735.
8. Sadek, F., Main, J.A., Lew, H.S., Robert, S.D., Chiarito, V.P., and El-Tawil, S. (2013) Performance of steel moment connections under a column removal scenario, I: experiments. *Journal of Structural Engineering*, **139**(1), 98-107.
9. Kanvinde, A.M. and Deierlein, G.G. (2004) *Micromechanical Simulation of Earthquake Induced Fracture in Steel Structures*. Blume Center TR 145. Stanford University, Stanford, CA.
10. Rice, J.R. and Tracey, D.M. (1969) On the ductile enlargement of voids in triaxial stress fields. *Journal of the Mechanics and Physics of Solids*, **17**(3), 201-217.
11. Hancock, J.W. and Mackenzie, A.C. (1976) On the mechanics of ductile failure in high-strength steel subjected to multi-axial stress-states. *Journal of Mechanics and Physics of Solids*, **24**(3), 147-169.
12. Kanvinde, A.M. and Deierlein, G.G. (2008) Validation of cyclic void growth model for fracture initiation in blunt notch and dogbone steel specimens. *J. Struct. Eng.*, 134(9), 1528-1537.
13. Kanvinde, A.M. and Deierlein, G.G. (2006) Void growth model and stress modified critical strain model to predict ductile fracture in structural steels. *J. Struct. Eng.*, **132**(12), 1907-18.
14. Kanvinde, A.M. and Deierlein, G.G. (2007) Cyclic void growth model to assess ductile fracture initiation in structural steels due to ultra low cycle fatigue. *J. Struct. Eng.*, **133**(6), 701-715.
15. Sadek, F., Main, J.A., Lew, H.S., Robert, S.D., Chiarito, V.P., and El-Tawil, S. (2010) *An Experimental and Computational Study of Steel Moment Connections under a Column Removal Scenario*. NIST Technical Note 1669, National Institute of Standards and Technology, U.S. Department of Commerce, Gaithersburg, Maryland.
16. Hibbitt, Karlsson and Sorensen Inc. (2014) *ABAQUS Standard User's Manual Version 14.1*. Providence.
17. Lee, P., Garai, R., and Ozkula, G. (2014) Issues on using welded built-up box columns in steel special moment frames. *Tenth U.S. National Conference on Earthquake Engineering Frontiers of Earthquake Engineering*, Anchorage, Alaska.

18. FEMA 350 (2000) *Interim Guidelines: Recommended Seismic Design Criteria for New Steel Moment-Frame Buildings*.

19. Kuwamura, H. and Yamamoto, K. (1997) Ductile crack as trigger of brittle fractures in steel. *J. Struct. Eng.*, **123**(6), 729-35.

20. Anderson, T.L. (2005) *Fracture Mechanics: Fundamentals and Applications*. 3rd ed. Boca Raton, FL: CRC Press.

21. Wang, Y., Zhou, H., Shi, Y. et al. (2011) Fracture prediction of welded steel connections using traditional fracture mechanics and calibrated micromechanics based models. *Int. J. Steel Struct.*, **11**, 351.

22. Zhou, H., Wang, Y., Shi, Y., Xiong, J., and Yang, L. (2013) Extremely low cycle fatigue prediction of steel beam-to-column connection by using a micro-mechanics based fracture model. *International Journal of Fatigue*, **48**, 90-100.

23. Zhou, H., Wang, Y., Yang, L., and Shi, Y. (2014) Seismic low-cycle fatigue evaluation of welded beam-to-column connections in steel moment frames through global-local analysis. *International Journal of Fatigue*, **64**, 97-113.

24. Saykin, V.V., Song, J., and Hajjar, J.F. (2014) *A Validated Approach to Modeling Collapse of Steel Structures. Department of Civil and Environmental Engineering Reports*. Report No. NEU-CEE-2014-02. Department of Civil and Environmental Engineering, Northeastern University, Boston, Massachusetts, http://hdl.handle.net/2047/d20014397.

25. Myers, A.T., Kanvinde, A.M., Deierlein, G.G., and Fell, B.V. (2009) Effect of weld details on the ductility of steel column baseplate connections. *Journal of Constructional Steel Research*, **65**(6), 1366-73.

26. Myers, AT., Deierlein, G.G., and Kanvinde, A.M. (2009) *Testing and Probabilistic Simulation of Ductile Fracture Initiation in Structural Steel Components and Weldments*. Blume Center TR 170. Stanford University, Stanford, CA.

27. Zhou, H. and Wang, Y. (2014) Seismic low-cycle fatigue evaluation of welded beam-to-column connections in steel moment frames through global-local analysis. *International Journal of Fatigue*, **64**, 97-113.

28. Benoit, A., Rémy, L., Koster, A., Maitournam, H., and Oger, F. (2014) Experimental investigation of the behavior and the low cycle fatigue life of a welded structure. *Materials Science and Engineering*, A, **595**, 64-76.

29. Hanji, T. (2014) Low cycle fatigue assessments of corner welded joints based on local strain approach. *International Journal of Steel Structures*, **14**(3), 579-587.

30. Zambrano, A. (2014) Damage indices evaluation for seismic resistant structures subjected to low-cycle fatigue phenomena. *International Journal of Mechanical Sciences*, **78**, 106-117.

31. Zarei, A. and Gerami, M. (2014) *Effect of low Cycle Fatigue on Steel Moment Frames with Prequalified Rigid Connections (Bolted Unstiffened and Stiffened Extended End-Plate Moment Connections)*. Faculty of Civil Engineering of Semnan University, Master's Thesis.

32. Tehranizadeh, M., Deylami, A., Gholami, M., and Moazemi, H. (2012) Validation of cyclic void growth model for fracture initiation in the flange plate connection between beam and box column. *15WCEE*, USBOA.

33. Ghaderi, M., Gerami, M., and Vahdani, M. (2019) A comparison of seismic low cycle fatigue and extremely low cycle fatigue on steel moment frames with reduced beam section connection (RBS). *International Journal of Fatigue*, **119**, 139-149.

34. ANSI/AISC 358-16. (2016) *Prequalified Connections for Special and Intermediate Steel Moment Frames for Seismic Applications*.

35. Ghaderi, M., Gerami, M., and Vahdani, R. (2020) Performance assessment of bolted extended end-plate moment connections constructed from grade St-37 steel subjected to fatigue. *Journal of Materials in Civil Engineering*, **32**(5), 1-15.

36. Gerami, M., Zarei, A., and Ghaderi, M. (2018)

Effect of low cycle fatigue on steel moment frames with prequalified rigid connections (bolted unstiffened and stiffened extended end-plate moment connections). *Journal of Structural and Construction Engineering (JSCE)*.

37. Ghaderi, M., Gerami, M., and Vahdani, R. (2019) Investigating the effect of extremely low cyclic fatigue in steel moment frames with reduced beam section connections. *Journal of Structural and Construction Engineering (JSCE)*.

38. Ghaderi, M., Gerami, M., and Vahdani, R. (2020) Estimated ultimate capacity of RBS connections under monotonic and cyclic load using ductile fracture mechanism. *Sharif Journal of Civil Engineering*, **36.2**(1.2), 143-152.